Conformal Intelligent Reflecting Surfaces for 6G V2V Communications

Dario Tagliaferri, Marouan Mizmizi, Reza Aghazadeh Ayoubi,
Gian Guido Gentili and Umberto Spagnolini
Politecnico di Milano, Milan, Italy
E-mails:{dario.tagliaferri,marouan.mizmizi,reza.aghazadeh,gianguido.gentili,umberto.spagnolini}@polimi.it

2022 1st International Conference on 6G Networking (6GNet) | 978-1-6654-6763-6/22/$31.00 ©2022 IEEE | DOI: 10.1109/6GNet54646.2022.9830337

***Abstract*—In the upcoming 6G vehicular networks, connected and automated vehicles are expected to rely on beam-based millimeter-wave/sub-THz vehicle-to-vehicle (V2V) communication links to facilitate advanced bandwidth-demanding safety-critical applications. However, communication at these frequencies is impaired by dynamic blockers, which might limit the effective range and reliability of V2V links. A common countermeasure to the blockage consists of enriching the scattering environment. In this context, intelligent reflecting surfaces (IRS) enable the control of the environment through the novel paradigm of a smart radio environment. This paper proposes to mount fully passive pre-configured conformal IRS (C-IRS) on the curved shape of vehicles' body. We derive the closed-form phase pattern expression to compensate for the non-flat shape of cars' doors, mimicking the behavior of a perfectly flat mirror. Simulation results show the benefits of the proposed C-IRS design in a highway V2V scenario, where the average signal-to-noise ratio can be improved up to 20 dB in dense traffic conditions.**

***Index Terms*—Conformal IRS, 6G, V2V, relay**

I. Introduction

Vehicle-to-everything (V2X) communication technologies are expected to play a pivotal role in future autonomous driving systems. Millimeter-wave (mmWave) ($30 - 100$ GHz) and sub-THz (> 100 GHz) bands have been recently proposed for V2X to encounter the ever-growing demand for bandwidth [1]–[3]. Propagation at these frequencies is subject to higher path and penetration losses compared to current sub-6 GHz systems [4]. Blockage from dynamic obstacles becomes one of the main challenges, if not the most important, for massive practical V2X deployment. In particular, vehicle-to-vehicle (V2V) communication systems are severely affected by power losses from random vehicles interposing between transmitter (Tx) and receiver (Rx), that at 30 GHz amount to $10 - 20$ dB (single blocker) and up to 40 dB (multiple blockers), increasing with the frequency [5], [6].

Hence, blockage mitigation solutions are a currently interesting research area. Relay-based solutions represent one feasible possibility for V2V. The authors of [7] consider the usage of relays of opportunity in a pure V2V context, while [8] involves the infrastructure, e.g., roadside units or cellular base stations (BS), pushing for network densification. The corresponding cost, however, increase. A completely different approach consider emerging metasurface technologies, i.e., intelligent reflecting surfaces (IRS) [9]. IRS are made by fully passive (pre-configured) or nearly passive (reconfigurable) arrays of sub-wavelength sized elements whose complex reflection coefficient is controlled to manipulate the impinging wavefront and change the reflection angle [10], [11]. IRS reconfigurability provides flexible dynamic adaptation of incidence/reflection angles in high-mobility environments, at the price of a non-negligible dedicated control signaling between Tx, Rx, and the IRS to estimate and set the phase of each element. Relevant contributions on reconfigurable IRS for blockage management are [12]–[15]. Works [12], [13] propose an IRS-assisted handover scheme for blockage avoidance in a cellular scenario, where the BS shall dynamically reconfigure IRS phases according to the needs of multiple users. The authors assume the perfect channel state information at each IRS, which might not be affordable for dense vehicular networks, where the channel is rapidly time-varying. The authors of [15] address the deployment optimization of multiple IRS in a cellular system, showing the benefits when multiple IRS are strategically deployed. However, the quantification of the overall deployment cost and signaling overhead for configuration is not tackled in the paper. On the other hand, pre-configured IRS represent a fully passive solution when the deployment cost of reconfigurable IRS is excessive, or the incidence/reflection angles are not a-priori known and cannot be accurately estimated [16], [17].

The purpose of this paper is to address the blockage

Authorized licensed use limited to: Politecnico di Milano. Downloaded on March 30,2023 at 18:11:13 UTC from IEEE Xplore. Restrictions apply.

issue in V2V communications by lodging conformal IRS on car sides (car doors). Unlike aforementioned works, considering planar metasurfaces, the vehicle's body is a conformal surface, which cannot be approximated to EM flat at mmWave/sub-THz frequencies. Existing works on conformal metasurfaces target acoustic wave and light manipulation [18], [19], while the application to a V2V context is unexplored. We first derive the optimal phase pattern for arbitrarily shaped IRS as a function of desired incidence and reflection angles. Then, we propose a novel phase design for pre-configured and fully passive C-IRS, where the cylindrical shape can be regarded as a second-order approximation of the complex non-planar shape of car doors. In the proposed design, C-IRS are aimed at compensating for the non-flat shape of cars' doors by mimicking a perfectly flat mirror. Numerical results concerning a multi-lane highway V2V scenario at 60 GHz carrier frequency show that equipping vehicles with fully passive C-IRS leads to an average SNR gain of 20 dB in dense traffic conditions, compared to direct V2V link. As a matter of comparison, reconfigurable C-IRS yield an SNR gain above 30 dB, at the price of a higher cost and a non-negligible control signaling. The results justify the adoption of pre-configured and fully passive C-IRS in 6G vehicular networks.

Organization: The remainder of the paper is organized as follows: Section II describes the system and channel model, Section III outlines the proposed C-IRS design, Section IV validates the remarkable benefits from the adoption of C-IRS for a V2V scenario. Finally, Section V concludes the paper.

Notation: Bold upper- and lower-case letters describe matrices and column vectors. The (i,j)-th entry of matrix $\mathbf{A}$ is denoted by $[\mathbf{A}]_{(i,j)}$. Matrix transposition, conjugate transposition and Frobenius norm are respectively as $\mathbf{A}^{\mathrm{T}}$, $\mathbf{A}^{\mathrm{H}}$ and $\|\mathbf{A}\|_F$. $\mathrm{tr}\,(\mathbf{A})$ extracts the trace of $\mathbf{A}$. $\mathrm{diag}(\mathbf{A})$ denotes the extraction of the diagonal of $\mathbf{A}$, while $\mathrm{diag}(\mathbf{a})$ is the diagonal matrix given by vector $\mathbf{a}$. $\mathbf{I}_n$ is the identity matrix of size n. With $\mathbf{a} \sim \mathcal{CN}(\boldsymbol{\mu}, \mathbf{C})$ we denote a multi-variate circularly complex Gaussian random variable $\mathbf{a}$ with mean $\boldsymbol{\mu}$ and covariance $\mathbf{C}$. $\mathbb{E}[\cdot]$ is the expectation operator, while $\mathbb{R}$ and $\mathbb{C}$ stand for the set of real and complex numbers, respectively.

II. System Model

We consider the multi-lane highway vehicular scenario depicted in Fig. 1. Each vehicle is equipped with a half-wavelength spaced uniform linear array (ULA) with K antenna elements, and two C-IRS on both vehicle's sides. At a given time instant, the position of Tx and

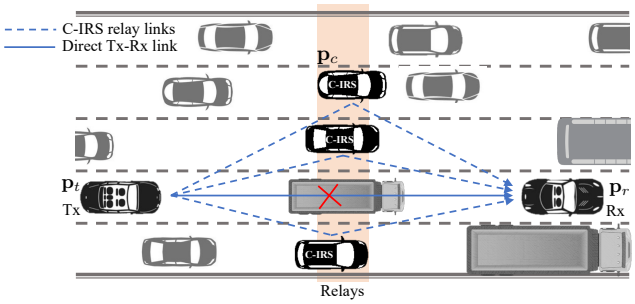

Fig. 1. Highway scenario: vehicles equipped with C-IRS can be used as passive and low-cost relays to reduce blockage affection.

Rx antennas is $\mathbf{p}_t = [x_t, y_t, z_t]^{\mathrm{T}}$ and $\mathbf{p}_r = [x_r, y_r, z_r]^{\mathrm{T}}$, respectively, defined in a global coordinate system. Similarly, the relaying vehicle is located in $\mathbf{p}_c = [x_c, y_c, z_c]^{\mathrm{T}}$, where $\mathbf{p}_c$ identifies the position of a reference element of the C-IRS. The global coordinate system is illustrated in Fig. 2. We assume the shape of each C-IRS along the door as cylindrical with a curvature radius R. In general, a car door has an arbitrarily complex shape; however, the cylindrical assumption allows for a closed-form analytical solution and to generalize the solution of planar IRS ($R \to \infty$) (see Fig. 3). In this setting, M elements of the C-IRS are deployed along the curved coordinate (height), and N elements along the cylindrical direction (length), for a total of $M \times N$ elements. The equipment is sketched in Fig. 2, where the length of the car's door is L and the height is H. The position of the (m,n)-th C-IRS element, for $m = -M/2, \ldots, M/2-1$ and $n = 0, \ldots, N-1$, is $\mathbf{p}_{m,n} = \mathbf{p}_c + [x_{m,n},\, y_{m,n},\, z_{m,n}]^{\mathrm{T}}$, where

$$\begin{aligned} x_{m,n} &= R\,(\cos\psi_m - 1) \\ y_{m,n} &= d_n(n-1) \\ z_{m,n} &= R\,\sin\psi_m \end{aligned} \tag{1}$$

denote the relative 3D displacement of the (m,n)-th element with respect to the reference one. Here, $\psi_m = 2m \arcsin\left(d_m/2/R\right)$ is the angular position in cylindrical coordinates of the m-th row, while d_m and d_n are the elements' spacing along the vertical and horizontal directions, respectively. For a reference car door height and length of $H = 1$ m and $L = 1$ m, selecting $R \in [2, 8]$ m provides a curvature that is in line with common car doors [20].

A. Signal and Channel Model

Let the complex transmitted symbol be $s \in \mathbb{C} \sim \mathcal{CN}\left(0, \sigma_s^2\right)$, where σ_s^2 is the transmitted power. Symbol

Authorized licensed use limited to: Politecnico di Milano. Downloaded on March 30,2023 at 18:11:13 UTC from IEEE Xplore. Restrictions apply.

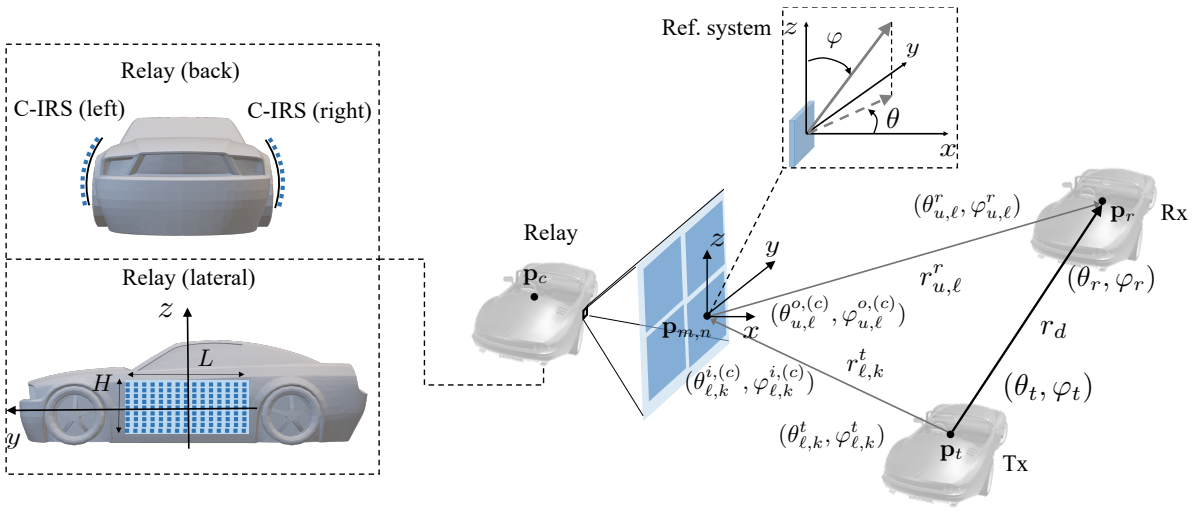

Fig. 2. Sketch of the geometry and the reference system of the considered V2V scenario. Vehicles are equipped with C-IRS on both lateral sides to serve as relays.

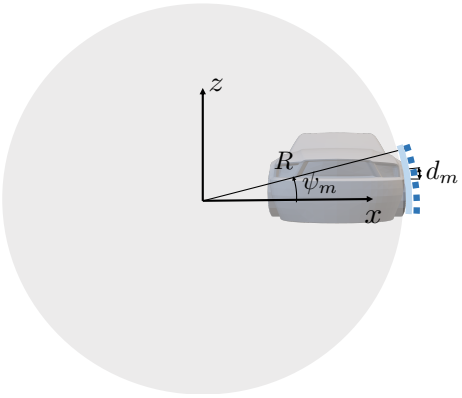

Fig. 3. Sketch of the cylindrical approximation of the car doors

s is beamformed by $\mathbf{f} \in \mathbb{C}^{K\times 1}$, propagates over a block-faded spatially-sparse channel $\mathbf{H} \in \mathbb{C}^{K\times K}$, the received signal is

$$y = \mathbf{w}^{\mathrm{H}}\mathbf{H}\mathbf{f}\, s + \mathbf{w}^{\mathrm{H}}\mathbf{n}, \tag{2}$$

where $\mathbf{w} \in \mathbb{C}^{K\times 1}$ is the Rx beamformer, and $\mathbf{n} \sim \mathcal{CN}\left(\mathbf{0}, \sigma_n^2\mathbf{I}_K\right)$ is the additive white Gaussian noise at the Rx antennas, with power σ_n^2.

The channel matrix in (2) is the sum of two contributions [21]:

$$\mathbf{H} = \mathbf{H}_d + \mathbf{H}_{cr}\mathbf{\Phi}\mathbf{H}_{tc} \tag{3}$$

where the first term $\mathbf{H}_d$ is the direct Tx-Rx link and the second term is via the C-IRS. Specifically, $\mathbf{H}_{tc} \in \mathbb{C}^{MN\times K}$ is the Tx-C-IRS channel for the incident signal, $\mathbf{H}_{cr} \in \mathbb{C}^{K\times MN}$ is the C-IRS-Rx channel for the reflected signal, and $\mathbf{\Phi} \in \mathbb{C}^{MN\times MN}$ is the complex reflection matrix (amplitude and phase) of the C-IRS.

As customary in mmWave/sub-THz communications, the channel (3) exhibits a sparse scattering characteristic [3]. The model for the direct channel $\mathbf{H}_d$ can be written for the far-field assumption, that typically applies for TxV-RxV distances in the order of tens of meters, as:

$$\mathbf{H}_d = \alpha_d\, \varrho_r(\boldsymbol{\vartheta}^r_d)\varrho_t(\boldsymbol{\vartheta}^t_d)\mathbf{a}_r(\boldsymbol{\vartheta}^r_d)\mathbf{a}_t(\boldsymbol{\vartheta}^t_d)^{\mathrm{H}} \tag{4}$$

where *(i)* α_d denotes the complex gain of the direct path, modelled as in [22]; *(ii)* $\mathbf{a}_t(\boldsymbol{\vartheta}^t_d) \in \mathbb{C}^{K\times 1}$, $\mathbf{a}_r(\boldsymbol{\vartheta}^r_d) \in \mathbb{C}^{K\times 1}$ are the Tx and Rx array response vectors, function of the angles of arrival (AoAs) and angles of departure (AoDs) of the direct path, respectively $\boldsymbol{\vartheta}^r_d = (\theta^r_d, \varphi^r_d)$ and $\boldsymbol{\vartheta}^t_d = (\theta^t_d, \varphi^t_d)$ (for azimuth and elevation), *(iv)* $\varrho_t(\boldsymbol{\vartheta}^t_d)$ and $\varrho_t(\boldsymbol{\vartheta}^r_d)$ are the Tx and Rx single-antenna gains, respectively. Similarly, the (ℓ, k)-th and (u, ℓ)-th entries of channel matrices $\mathbf{H}_{tc}$ and $\mathbf{H}_{cr}$, for $\ell = (m-1)M+n$, $u, k = 1, ..., K$ can be written under the far field assumption as

$$\begin{aligned}
[\mathbf{H}_{tc}]_{(\ell,k)} &= \alpha_{\ell,k}\; \varrho_t(\boldsymbol{\vartheta}_t)\, \varrho_c(\boldsymbol{\vartheta}^{i,(c)}_{\ell,k})\, e^{-j\frac{2\pi}{\lambda}r^t_{\ell,k}} \\
[\mathbf{H}_{cr}]_{(u,\ell)} &= \alpha_{u,\ell}\; \varrho_c(\boldsymbol{\vartheta}^{o,(c)}_{u,\ell})\varrho_r(\boldsymbol{\vartheta}_r)\, e^{-j\frac{2\pi}{\lambda}r^r_{u,\ell}}
\end{aligned} \tag{5}$$

where *(i)* $\alpha_{\ell,k}$ and $\alpha_{u,\ell}$ are the complex gains of the path between the k-th Tx antenna and the ℓ-th C-IRS element and between the ℓ-th C-IRS element and the u-th Rx antenna, respectively [22]; *(ii)* $\boldsymbol{\vartheta}_t$ and $\boldsymbol{\vartheta}_r$ are the AoD and AoA to/from the C-IRS, respectively; *(iii)* $r^t_{\ell,k}$ and $r^r_{u,\ell}$ are the propagation distances; *(iv)* $\varrho_c(\cdot)$ is the C-IRS element pattern, function of the *local* angles of incidence and reflection (AoI, AoR) $\boldsymbol{\vartheta}^{i,(c)}_{\ell,k}$, $\boldsymbol{\vartheta}^{o,(c)}_{u,\ell}$, identified by superscript $^{(c)}$. Notice that local AoI/AoR can be expressed as function of the *global* ones $\boldsymbol{\vartheta}_i = (\theta_i, \varphi_i)$ and

Authorized licensed use limited to: Politecnico di Milano. Downloaded on March 30,2023 at 18:11:13 UTC from IEEE Xplore. Restrictions apply.

$\boldsymbol{\vartheta}_o = (\theta_o, \varphi_o)$ knowing the shape of the C-IRS. Herein, we assume the the widely employed model in [23] for $\varrho_t(\cdot)$, $\varrho_r(\cdot)$ and $\varrho_c(\cdot)$. The reflection matrix $\boldsymbol{\Phi}$ at the C-IRS in (3) is diagonal with entries defined as

$$\boldsymbol{\Phi} = \text{diag}\left(\beta_1 e^{j\Phi_1}, ..., \beta_\ell e^{j\Phi_\ell}, ..., \beta_{MN} e^{j\Phi_{MN}}\right) \quad (6)$$

where β_ℓ and Φ_ℓ denote the amplitude and phase of the ℓ-th element reflection coefficient, respectively. In the following, we assume the surface is made of a fully reflecting material (e.g., a metal); thus, there is no penetration and $|\beta_\ell| = 1 \ \forall \ell$.

III. Conformal IRS Design for V2V Communications

A. Generalized Reflection's Law

Let us consider the reference system depicted in Fig. 2, where a plane wave is impinging on a 3D reflecting surface $y = f(x, z)$ from an arbitrary direction. Incident and reflected wavevectors are

$$\mathbf{k} = -\frac{2\pi}{\lambda}\left[\sin\varphi_i \cos\theta_i,\ \sin\varphi_i \sin\theta_i,\ \cos\varphi_i\right]^{\mathrm{T}}, \quad (7)$$

$$\overline{\mathbf{k}} = \frac{2\pi}{\lambda}\left[\sin\varphi_o \cos\theta_o,\ \sin\varphi_o \sin\theta_o,\ \cos\varphi_o\right]^{\mathrm{T}} \quad (8)$$

Assuming there is a phase variation $\Phi(x, y, z)$ defined in the neighborhood of $y = f(x, z)$, the relation between $\mathbf{k}$ and $\overline{\mathbf{k}}$ is determined by the generalized Snell's law [24]:

$$\mathbf{k} - \overline{\mathbf{k}} = \nabla\Phi + \nu\mathbf{u} \quad (9)$$

where $\nu \in \mathbb{R}$ and $\mathbf{u}$ is the unit vector normal to the surface, defined as

$$\mathbf{u} = \frac{\left[-\frac{\partial f}{\partial x}, 1, -\frac{\partial f}{\partial z}\right]^{\mathrm{T}}}{\sqrt{1 + \|\nabla f\|^2}}. \quad (10)$$

Eq. (9) allows to derive the optimal phase pattern to be applied to an arbitrarily shaped metasurface to realize specular/anomalous reflection. It can be demonstrated that the phase to be applied across the surface to reflect an impinging wave from (θ_i, φ_i) toward (θ_o, φ_o) is reported in (11). By plugging the 3D position of the (m, n)-th C-IRS element into (11), namely setting $x = x_{m,n}$, $y = y_{m,n}$ and $z = z_{m,n}$ as in (1), we obtain the optimal phase configuration for any pair AoI/AoR, (θ_i, φ_i) and (θ_o, φ_o). Notice that the phase configuration (11) can be regarded as generalization of the planar one, since letting $R \to \infty$ implies $x_{m,n} \to 0$, $y_{m,n} \to d_n(n-1)$ and $z_{m,n} \to d_m(m-1)$, providing the conventional phase configuration for planar IRS [9].

B. Pre-configured C-IRS for Vehicular Applications

According to (11), the optimal usage of a C-IRS requires the knowledge of AoIs and AoRs, i.e., (θ_i, φ_i) and (θ_o, φ_o). However, the latter are rapidly time-varying in vehicular scenarios, and the direct usage of (11) implies the possibility to dynamically reconfigure $\boldsymbol{\Phi}$, with the well known penalty in terms of cost and signaling overhead. Therefore, we propose a novel phase design for a pre-configured, fully passive cylindrical-shaped C-IRS, that can be a local approximation of a portion of car lateral doors. The aim is to make the C-IRS to behave as a perfectly EM flat surface, i.e., a mirror, for specific azimuth and elevation angular intervals that match the typical AoIs and AoRs in vehicular networks.

We approach the C-IRS design by imposing a specular reflection in (11). Specifically, we leverage the empirical probability density functions (EPDFs) of azimuth and elevation AoI, θ_i and φ_i, in the same multi-lane highway scenario described in Section II. The EPDFs are shown in Figs. 4a and 4b, respectively, for $0 \leq \varphi_i \leq 90$ deg and $0 \leq \theta_i \leq 90$, obtained from through extensive traffic simulations based on SUMO [25] for different vehicle types, e.g., passenger cars, trucks, buses, etc., and locations. Since vehicles have similar heights compared to typical V2V distances (ranging from few to tens of meters), elevation AoI are mostly distributed around $\varphi_i = 90$ deg, within ≈ 1.5 deg ($\approx 67\%$ of AoI). Differently, the EPDF of azimuth AoI θ_i is wider and monotonically increases for $|\theta_i| \to 90$ deg, as shown in Fig. 4b. The azimuth variability is a consequence of the random vehicle positions in space (varying of tens of meters), that dominates over the height differences ruling the EPDF of φ_i (in the order of tens of centimeters to few meters). Therefore, we reasonably impose $\varphi_i = \varphi_o = 90$ deg and leave the azimuth as a free parameter $\theta_o = -\theta_i = \overline{\theta}$ in (11), obtaining the following phase pattern

$$\Phi_m(\overline{\theta}) = -\frac{4\pi R}{\lambda}\left(\cos\psi_m - 1\right)\cos\overline{\theta}, \quad (12)$$

that depends *only* on the shape of the C-IRS along the curved dimension, i.e., on curvature radius R and angular position of the elements $\{\psi_m\}$, as well as on the operating azimuth angle $\overline{\theta}$. Notice that the phase gradient is non-zero along the curved dimension only. According to the experienced azimuth AoI, $\overline{\theta}$ can be pre-configured to make the C-IRS work around the dominant region of the PDF, i.e., for $|\theta_i| \geq 45$ deg, thus $45 \leq \overline{\theta} \leq 90$ deg.

The impact of the phase configuration in (12) can be assessed by the azimuth normalized radiation pattern

Authorized licensed use limited to: Politecnico di Milano. Downloaded on March 30,2023 at 18:11:13 UTC from IEEE Xplore. Restrictions apply.

$$\Phi(x,y,z) = -\frac{2\pi}{\lambda}\left[x\left(\cos\theta_o \sin\varphi_o + \cos\theta_i \sin\theta_i\right) + y\left(\sin\theta_o \sin\varphi_o + \sin\theta_i \sin\varphi_i\right) + z\left(\cos\varphi_o + \cos\varphi_i\right)\right] \quad (11)$$

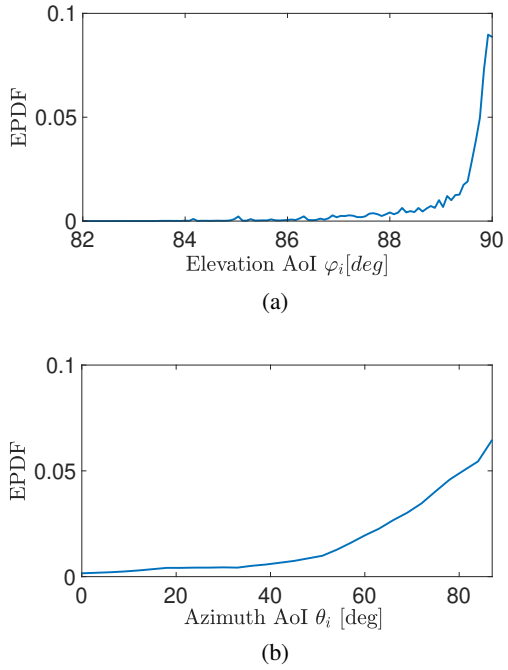

Fig. 4. EPDF of elevation (4a) and azimuth (4b) AoI in a typical multi-lane highway V2V scenario

$P(\theta|\overline{\theta})$ of the C-IRS for specular reflection, i.e., for $\varphi_i = \varphi_o = \pi/2$, $\theta_o = -\theta_i = \theta$ and fixed configuration parameter $\overline{\theta}$, defined as

$$\begin{aligned} P(\theta|\overline{\theta}) &= \left|\frac{1}{M}\sum_m e^{-j\Phi_m(\theta)} e^{j\Phi_m(\overline{\theta})}\right|^2 = \\ &= \left|\frac{1}{M}\sum_m e^{-j\frac{4\pi R}{\lambda}(\cos\psi_m - 1)(\cos\theta - \cos\overline{\theta})}\right|^2 = \\ &= \left|e^{j\beta}\left[J_0(\beta) - jH_0(\beta)\right]\right|^2, \end{aligned} \quad (13)$$

where $\beta = (4\pi R/\lambda)(\cos\theta - \cos\overline{\theta})$, $J_0(\beta)$ is the Bessel 0 function of the first kind [26], and $H_0(\beta)$ is the Struve function [27]. We consider $f = 60$ GHz as operating frequency ($\lambda = 5$ mm wavelength), a C-IRS area of 1 m^2 (corresponding to $M = 800$ and $N = 800$ elements at $d_n = d_m = \lambda/4$ spacing). Fig. 5a depicts the C-IRS pattern $P(\theta|\overline{\theta})$ for different values of the configuration parameter $\overline{\theta}$, for $R = 8$ m. Fixing $\overline{\theta}$, the angular response of the C-IRS for specular reflection is selective in θ. Hence, C-IRS provides the desired

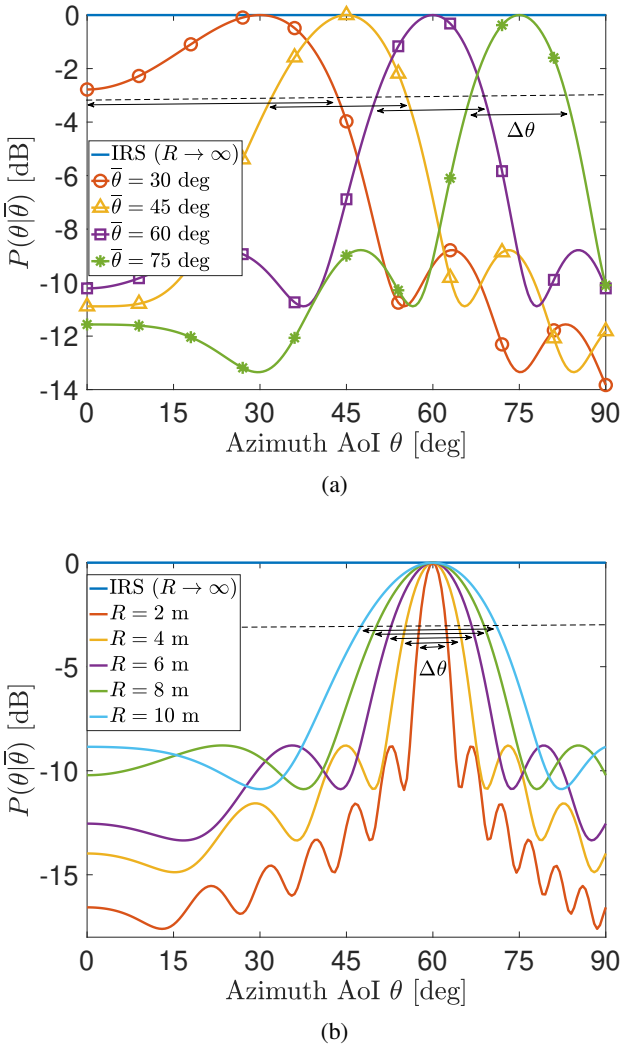

Fig. 5. Specular normalized C-IRS pattern as function of (5a) configuration parameter $\overline{\theta}$ ($R = 8$ m); (5b) radius of curvature R ($\overline{\theta} = 60$ deg), compared to a flat IRS ($R \to \infty$).

specular reflection for $\theta_i \in [\overline{\theta} - (\Delta\theta/2), \overline{\theta} + (\Delta\theta/2)]$, where $\Delta\theta$ is the angular interval for which the C-IRS reflects optimally. We also notice that, for increasing $\overline{\theta}$, the angular interval for specular reflection $\Delta\theta$ gets narrower. In particular, $\Delta\theta \approx 45$ deg for $\overline{\theta} = 30$ deg and $\Delta\theta \approx 17$ deg for $\overline{\theta} = 75$ deg. The trend of $P(\theta|\overline{\theta})$ varying the curvature radius of the C-IRS R is in Fig. 5b. As expected, the more the cylindrical surface tends to a flat surface ($R \to \infty$), the larger is the angular interval of specular reflection $\Delta\theta$. For $\overline{\theta} = 60$ deg, $\Delta\theta$

Authorized licensed use limited to: Politecnico di Milano. Downloaded on March 30,2023 at 18:11:13 UTC from IEEE Xplore. Restrictions apply.

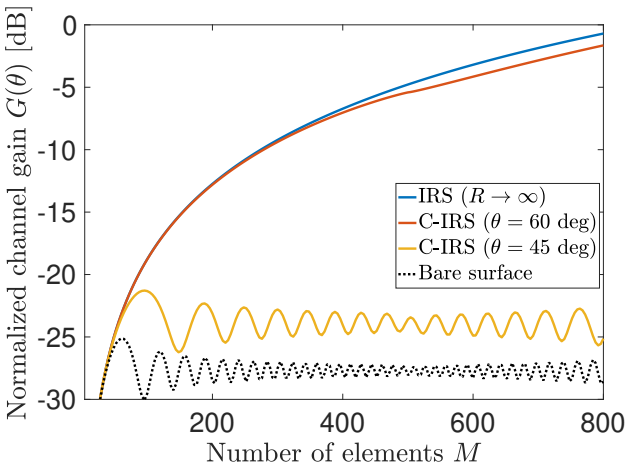

Fig. 6. Specular normalized channel gain on the azimuth plane for a C-IRS compared to a flat IRS ($R \to \infty$) and a bare cylindrical surface (i.e., without phase compensation) varying the number of elements M

ranges from 25 deg ($R = 10$ m) to 5 deg ($R = 2$ m). Considering the EPDF of the azimuth AoI θ_i, the proper working condition of C-IRS in a V2V scenario with highly curved car doors can be set either with a proper tuning of $\overline{\theta}$, including the majority of experienced azimuth AoI, or by reducing the number of elements M along the conformal coordinate (thus the overall gain) in favor of a wider angular aperture for specular reflection. To this aim, we assess the normalized azimuth channel gain $G(\theta)$, defined as

$$G(\theta) = \mathrm{tr}\left(\mathbf{H}_{cr} \mathbf{\Phi} \mathbf{H}_{tc} \mathbf{H}_{tc}^{\mathrm{H}} \mathbf{\Phi}^{\mathrm{H}} \mathbf{H}_{cr}^{\mathrm{H}} \Big|_{\substack{\varphi_i = \varphi_o = \frac{\pi}{2} \\ \theta_o = -\theta_i = \theta}} \right) \quad (14)$$

where: $\mathbf{H}_{tc}$ and $\mathbf{H}_{cr}$ are from (5) and normalized such that $\|\mathbf{H}_{tc}\|_F = \|\mathbf{H}_{cr}\|_F = 1$ and $\|\mathbf{\Phi}\|_F = 1/M_{\max}$, where $M_{\max}$ is the maximum number of considered elements across the conformal direction. $G(\theta)$ is thus independent from specific Tx-C-IRS and C-IRS-Rx distances. Fig. 6 shows the trend of $G(\theta)$ varying M, for $R = 8$ m, $\overline{\theta} = 60$ deg, and $M_{\max} = 800$, comparing the behavior of C-IRS, flat IRS ($R \to \infty$) and a bare cylindrical surface (without phase compensation). The first observation is that a properly configured C-IRS systematically provides a channel gain gap compared to a bare surface. In particular, the gap is in excess of 25 dB for $M = 800$ (thus $H = 1$ m side). When $\theta \neq \overline{\theta}$, instead, increasing M does not lead to a due increase in the channel gain, as the phase pattern is optimized for $\overline{\theta}$ only. However, reducing M allows to diminish the gap between $G(\overline{\theta})$ and $G(\theta)$, hence increasing $\Delta\theta$, at the price of a lower maximum achievable gain.

TABLE I
SIMULATION PARAMETERS

Parameter	Symbol	Value(s)
Carrier frequency	f	60 GHz
Number of Tx/Rx antennas	K	8
Tx-Rx distance	r_d	100 m
Number of C-IRS elements	$M \times N$	800×800 ($1\mathrm{m}^2$ area)
C-IRS element spacing	d_m, d_n	$\lambda/4$
C-IRS curvature radius	R	8 m
C-IRS configuration param.	$\overline{\theta}$	75 deg
Transmitted power	σ_s^2	10 dBm
Noise power	σ_n^2	-88 dBm

IV. NUMERICAL RESULTS

This section shows the advantages of equipping vehicles with C-IRS on lateral sides. We consider as a case study, a multi-lane highway road segment of 500 m length with $N_l = 5$ lanes, each of $w_l = 5$ m width. The Tx-Rx distance is set to $r_d = 100$ m, and all the other vehicles are randomly distributed on each lane according to a point Poisson process [28] with a traffic density ρ cars/km (per lane). All vehicles in the scenario are modelled with an occupation region of $5 \times 1.8 \times 1.5$ m^3. The system and communication parameters used in the simulations are summarized in Table I.

Let us assume that Tx and Rx know their positions, namely $\mathbf{p}_t$ and $\mathbf{p}_r$, as well as the position of neighboring CAVs. For instance, position information can be obtained through signaling or sensing [29], [30]. When vehicles are equipped with pre-configured C-IRS on their sides, designed for specular reflection, the optimal relaying vehicle, in position $\mathbf{p}_c$, is located halfway between Tx and Rx, within a region of size $A_s = W_s \times L_s$ centered in $(\mathbf{p}_r - \mathbf{p}_t)/2$. While $W_s = N_l w_l$ is the highway width, L_s is chosen to be two times the length of the C-IRS, i.e., $L_s = 2L$. The Tx and Rx beamformers $\mathbf{f}$ and $\mathbf{w}$ in (2) are chosen from beamforming codebooks $\mathcal{F}$ and $\mathcal{W}$ built upon the knowledge of the Tx, Rx and candidate relay positions within area A_s. Considering the position of the c-th relay, $\mathbf{p}_c$, the corresponding Tx and Rx beamforming vectors are:

$$\mathbf{f}_c = \left[1, ..., e^{-j\pi(K-1)\cos\theta_t}\right]^{\mathrm{T}} \quad (15)$$

$$\mathbf{w}_c = \left[1, ..., e^{-j\pi(K-1)\cos\theta_r}\right]^{\mathrm{T}} \quad (16)$$

Authorized licensed use limited to: Politecnico di Milano. Downloaded on March 30,2023 at 18:11:13 UTC from IEEE Xplore. Restrictions apply.

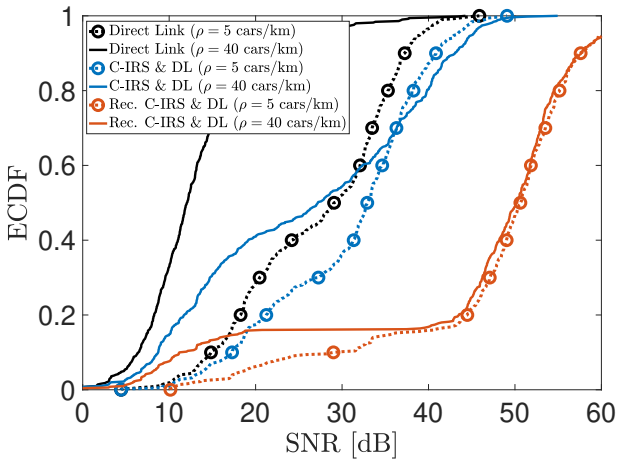

(a)

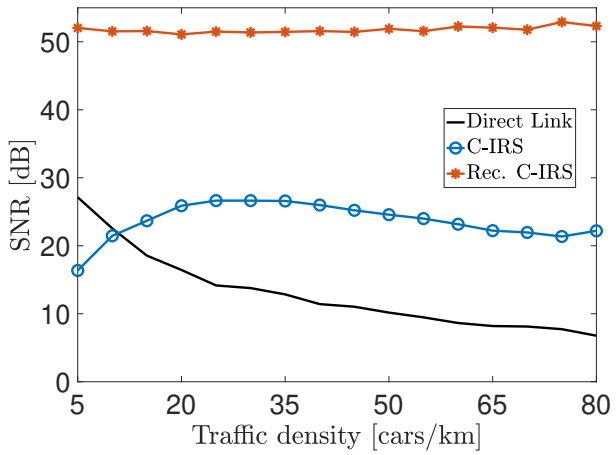

(b)

Fig. 7. (7a) ECDF of the SNR employing direct V2V link only, fully passive and pre-configured C-IRS, reconfigurable C-IRS, varying the traffic density; (7b) average SNR as function of the traffic density

for azimuth angles

$$\theta_t = \arctan\left(\frac{y_c - y_t}{x_c - x_t}\right), \ \theta_r = \arctan\left(\frac{y_r - y_c}{x_r - x_c}\right). \tag{17}$$

Therefore, the beam codebooks are defined as

$$\mathcal{F} = \{\mathbf{f}_d, \{\mathbf{f}_c\}\}, \qquad \mathcal{W} = \{\mathbf{w}_d, \{\mathbf{w}_c\}\} \tag{18}$$

where $\mathbf{f}_d$ and $\mathbf{w}_d$ denote the beamforming vectors for the direct Tx-Rx link. Beamforming vectors $\mathbf{f}$ and $\mathbf{w}$ in (2) are chosen as the maximizers of the SNR, i.e.,

$$\mathbf{f}_{opt}, \mathbf{w}_{opt} = \underset{\substack{\mathbf{f}\in\mathcal{F} \\ \mathbf{w}\in\mathcal{W}}}{\text{argmax}} \left\{ \frac{\sigma_s^2 |\mathbf{w}^{\text{H}}\mathbf{H}\mathbf{f}|^2}{K\sigma_n^2} \right\}. \tag{19}$$

The results are summarized by Fig. 7. Fig. 7a shows the empirical cumulative distribution function (ECDF) of the SNR for $\rho = 5$ cars/km and $\rho = 40$ cars/km, when using: direct link only (black lines), pre-configured C-IRS and direct link (according to (18) and (19), blue lines), reconfigurable C-IRS and direct link (red lines). In the latter case, we assume an instantaneous real-time phase reconfiguration of the C-IRS according to a perfect channel knowledge. We notice that fully passive and pre-configured provide a substantial SNR gain in both low and high traffic conditions. The average SNR gap compared to the usage of the direct Tx-Rx link ranges from 5 dB to 20 dB, respectively, and increases with ρ. Fig. 7b shows the trend of the average SNR using either the direct link or the link via the C-IRS. For $\rho > 10$ cars/km, the usage of pre-configured C-IRS becomes advantageous: increasing ρ leads to an increase of the blockage probability of the direct link, and the benefits of a fully passive relaying vehicle is evident. As a matter of comparison, reconfigurable C-IRS allows for much higher SNR gap, in excess of $20 - 40$ dB, thanks to the flexibility with respect to the AoI/AoR, that increases the number of vehicles potentially serving as relays. However, the intensive signaling to estimate the channel and configure the C-IRS might be overwhelming for V2V, indicating the fully passive and pre-configured design as a promising and viable solution for 6G vehicular networks.

V. Conclusion

With the advent of self-driving cars, vehicles are expected to reliably share massive amounts of data with neighbors via highly directional mmWave/sub-THz beam-based V2V links for a wide range of vehicular services. In this setting, however, blockage from random vehicles drastically reduces the reliability of V2V links. This paper proposes using conformal-designed IRS deployed on vehicles' doors as passive relays in mmWave/sub-THz vehicular networks. In particular, a novel phase design for non-reconfigurable fully passive C-IRS is proposed to compensate for the non-flat door's shape. Numerical simulations at 60 GHz carrier frequency in a highway scenario show a remarkable improvement of average SNR in dense traffic conditions, about 20 dB when using fully passive and non-reconfigurable C-IRS. Future investigation will concern other scenarios and optimal pre-configuration patterns.

Acknowledgment

The work has been partially supported by the Huawei-Politecnico di Milano Joint Research Lab.

Authorized licensed use limited to: Politecnico di Milano. Downloaded on March 30,2023 at 18:11:13 UTC from IEEE Xplore. Restrictions apply.

REFERENCES

[1] 3GPP, "Study on channel model for frequencies from 0.5 to 100 ghz (release 16, tr 22186)," 2019.

[2] ——, "Enhancement of 3gpp support for v2x scenarios (tr 22186)," 2019.

[3] T. S. Rappaport, Y. Xing, O. Kanhere, S. Ju, A. Madanayake, S. Mandal, A. Alkhateeb, and G. C. Trichopoulos, "Wireless communications and applications above 100 ghz: Opportunities and challenges for 6g and beyond," *IEEE access*, vol. 7, pp. 78 729–78 757, 2019.

[4] F. Jameel, S. Wyne, S. J. Nawaz, and Z. Chang, "Propagation channels for mmwave vehicular communications: State-of-the-art and future research directions," *IEEE Wireless Communications*, vol. 26, no. 1, pp. 144–150, 2018.

[5] J.-J. Park, J. Lee, J. Liang, K.-W. Kim, K.-c. Lee, and M.-D. Kim, "Millimeter wave vehicular blockage characteristics based on 28 ghz measurements," in *2017 IEEE 86th Vehicular Technology Conference (VTC-Fall)*. IEEE, 2017, pp. 1–5.

[6] K. Dong, M. Mizmizi, D. Tagliaferri, and U. Spagnolini, "Vehicular blockage modelling and performance analysis for mmwave v2v communications," *arXiv preprint arXiv:2110.10576*, 2021.

[7] F. Linsalata, S. Mura, M. Mizmizi, M. Magarini, P. Wang, M. N. Khormuji, A. Perotti, and U. Spagnolini, "Los-map construction for proactive relay of opportunity selection in 6g v2x systems," *arXiv preprint arXiv:2111.07804*, 2021.

[8] I. K. Jain, R. Kumar, and S. S. Panwar, "The impact of mobile blockers on millimeter wave cellular systems," *IEEE Journal on Selected Areas in Communications*, vol. 37, no. 4, pp. 854–868, 2019.

[9] Y. Liu, X. Liu, X. Mu, T. Hou, J. Xu, M. Di Renzo, and N. Al-Dhahir, "Reconfigurable intelligent surfaces: Principles and opportunities," *IEEE Communications Surveys Tutorials*, vol. 23, no. 3, pp. 1546–1577, 2021.

[10] Y. Zhang, J. Zhang, M. Di Renzo, H. Xiao, and B. Ai, "Performance analysis of ris-aided systems with practical phase shift and amplitude response," *IEEE Transactions on Vehicular Technology*, 2021.

[11] G. Oliveri, P. Rocca, M. Salucci, and A. Massa, "Holographic smart em skins for advanced beam power shaping in next generation wireless environments," *arXiv preprint arXiv:2106.10932*, 2021.

[12] Y. Chen, Y. Wang, J. Zhang, and M. Di Renzo, "Qos-driven spectrum sharing for reconfigurable intelligent surfaces (riss) aided vehicular networks," *IEEE Transactions on Wireless Communications*, 2021.

[13] L. Jiao, P. Wang, A. Alipour-Fanid, H. Zeng, and K. Zeng, "Enabling efficient blockage-aware handover in ris-assisted mmwave cellular networks," *IEEE Transactions on Wireless Communications*, pp. 1–1, 2021.

[14] G. Zhou, C. Pan, H. Ren, K. Wang, M. D. Renzo, and A. Nallanathan, "Robust beamforming design for intelligent reflecting surface aided miso communication systems," *IEEE Wireless Communications Letters*, vol. 9, no. 10, pp. 1658–1662, 2020.

[15] Y. U. Ozcan, O. Ozdemir, and G. K. Kurt, "Reconfigurable intelligent surfaces for the connectivity of autonomous vehicles," *IEEE Transactions on Vehicular Technology*, vol. 70, no. 3, pp. 2508–2513, 2021.

[16] S. Sahin, N. K. Nahar, and K. Sertel, "Dielectric Properties of Low-Loss Polymers for mmW and THz Applications," *Journal of Infrared, Millimeter, and Terahertz Waves*, vol. 40, pp. 557–573, 2019.

[17] I. Cherukhin, S.-P. Gao, and Y. Guo, "Fully Flexible Polymer-Based Microwave Devices: Materials, Fabrication Technique, and Application to Transmission Lines," *IEEE Transactions on Antennas and Propagation*, vol. 69, no. 12, pp. 8763–8777, 2021.

[18] X.-S. Li, Y.-F. Wang, A.-L. Chen, and Y.-S. Wang, "An arbitrarily curved acoustic metasurface for three-dimensional reflected wave-front modulation," *Journal of Physics D: Applied Physics*, vol. 53, no. 19, p. 195301, 2020.

[19] L. La Spada, C. Spooner, S. Haq, and Y. Hao, "Curvilinear metasurfaces for surface wave manipulation," *Scientific reports*, vol. 9, no. 1, pp. 1–10, 2019.

[20] L. Fan, J. Xiaomin, H. Gang, and G. Jing, "A novel shape-adjustable surface and its applications in car design," *Journal of Applied Science*, vol. 9, no. 2339, pp. 1–20, 2019.

[21] E. Björnson and L. Sanguinetti, "Rayleigh fading modeling and channel hardening for reconfigurable intelligent surfaces," *IEEE Wireless Communications Letters*, vol. 10, no. 4, pp. 830–834, 2021.

[22] 3rd Generation Partnership Project (3GPP), "Study on evaluation methodology of new vehicle-to-everything (v2x) use cases for lte and nr (v15.3.0, release 15)," vol. TR 37.885, Tech. Rep., 2019.06.

[23] S. W. Ellingson, "Path loss in reconfigurable intelligent surface-enabled channels," in *2021 IEEE 32nd Annual International Symposium on Personal, Indoor and Mobile Radio Communications (PIMRC)*, 2021, pp. 829–835.

[24] S. R. Biswas, C. E. Gutiérrez, A. Nemilentsau, I.-H. Lee, S.-H. Oh, P. Avouris, and T. Low, "Tunable graphene metasurface reflectarray for cloaking, illusion, and focusing," *Phys. Rev. Applied*, vol. 9, p. 034021, Mar 2018. [Online]. Available: https://link.aps.org/doi/10.1103/PhysRevApplied.9.034021

[25] P. A. Lopez, M. Behrisch, L. Bieker-Walz, J. Erdmann, Y.-P. Flötteröd, R. Hilbrich, L. Lücken, J. Rummel, P. Wagner, and E. Wießner, "Microscopic Traffic Simulation using SUMO," in *The 21st IEEE International Conference on Intelligent Transportation Systems*. IEEE, 2018. [Online]. Available: https://elib.dlr.de/124092/

[26] G. N. Watson, *A treatise on the theory of Bessel functions*. Cambridge university press, 1995.

[27] J. Newman, "Approximations for the bessel and struve functions," *Mathematics of Computation*, vol. 43, no. 168, pp. 551–556, 1984.

[28] A. Abul-Magd, "Modeling highway-traffic headway distributions using superstatistics," *Physical Review E*, vol. 76, no. 5, p. 057101, 2007.

[29] D. Tagliaferri, M. Brambilla, M. Nicoli, and U. Spagnolini, "Sensor-aided beamwidth and power control for next generation vehicular communications," *IEEE Access*, vol. 9, pp. 56 301–56 317, 2021.

[30] M. Brambilla, M. Nicoli, G. Soatti, and F. Deflorio, "Augmenting vehicle localization by cooperative sensing of the driving environment: Insight on data association in urban traffic scenarios," *IEEE Transactions on Intelligent Transportation Systems*, vol. 21, no. 4, pp. 1646–1663, 2020.

Authorized licensed use limited to: Politecnico di Milano. Downloaded on March 30,2023 at 18:11:13 UTC from IEEE Xplore. Restrictions apply.